

An immunogenic personal neoantigen vaccine for patients with melanoma

Patrick A. Ott^{1,2,3*}, Zhuting Hu^{1*}, Derin B. Keskin^{1,3,4}, Sachet A. Shukla^{1,4}, Jing Sun¹, David J. Bozym¹, Wandu Zhang¹, Adrienne Luoma⁵, Anita Giobbie-Hurder⁶, Lauren Peter^{7,8}, Christina Chen¹, Oriol Olive¹, Todd A. Carter⁴, Shuqiang Li⁴, David J. Lieb⁴, Thomas Eisenhaure⁴, Evisa Gjini⁹, Jonathan Stevens¹⁰, William J. Lane¹⁰, Indu Javeri¹¹, Kaliappanadar Nellaiappan¹¹, Andres M. Salazar¹², Heather Daley¹, Michael Seaman⁷, Elizabeth I. Buchbinder^{1,2,3}, Charles H. Yoon^{3,13}, Maegan Harden⁴, Niall Lennon⁴, Stacey Gabriel⁴, Scott J. Rodig^{9,10}, Dan H. Barouch^{3,7,8}, Jon C. Aster^{3,10}, Gad Getz^{3,4,14}, Kai Wucherpfennig^{3,5}, Donna Neuberg⁶, Jerome Ritz^{1,2,3}, Eric S. Lander^{3,4}, Edward F. Fritsch^{1,4†}, Nir Hacohen^{3,4,15} & Catherine J. Wu^{1,2,3,4}

Effective anti-tumour immunity in humans has been associated with the presence of T cells directed at cancer neoantigens¹, a class of HLA-bound peptides that arise from tumour-specific mutations. They are highly immunogenic because they are not present in normal tissues and hence bypass central thymic tolerance. Although neoantigens were long-envisioned as optimal targets for an anti-tumour immune response², their systematic discovery and evaluation only became feasible with the recent availability of massively parallel sequencing for detection of all coding mutations within tumours, and of machine learning approaches to reliably predict those mutated peptides with high-affinity binding of autologous human leukocyte antigen (HLA) molecules. We hypothesized that vaccination with neoantigens can both expand pre-existing neoantigen-specific T-cell populations and induce a broader repertoire of new T-cell specificities in cancer patients, tipping the intra-tumoural balance in favour of enhanced tumour control. Here we demonstrate the feasibility, safety, and immunogenicity of a vaccine that targets up to 20 predicted personal tumour neoantigens. Vaccine-induced polyfunctional CD4⁺ and CD8⁺ T cells targeted 58 (60%) and 15 (16%) of the 97 unique neoantigens used across patients, respectively. These T cells discriminated mutated from wild-type antigens, and in some cases directly recognized autologous tumour. Of six vaccinated patients, four had no recurrence at 25 months after vaccination, while two with recurrent disease were subsequently treated with anti-PD-1 (anti-programmed cell death-1) therapy and experienced complete tumour regression, with expansion of the repertoire of neoantigen-specific T cells. These data provide a strong rationale for further development of this approach, alone and in combination with checkpoint blockade or other immunotherapies.

To generate a vaccine that targets personal neoantigens, we conducted whole-exome sequencing (WES) of matched tumour- and normal-cell DNA from individual patients, identified somatic mutations, orthogonally validated and assessed the expression of mutated alleles by RNA sequencing (RNA-seq) of the tumour, predicted which mutated peptides were likely to bind autologous HLA-A or HLA-B proteins of the patient, and synthesized clinical-grade long peptides³ targeting up to 20 neoantigens per patient, admixed with the Toll-like receptor 3 (TLR3) and melanoma differentiation-associated protein 5 (MDA-5)

agonist poly-ICLC⁴ (Hiltonol) (Fig. 1a and Supplementary Information 1–3). We evaluated this vaccine in a phase I study in patients with previously untreated high-risk melanoma (stage IIIB/C and IVM1a/b) after surgical resection with curative intent (Extended Data Table 1 and Supplementary Information 4a).

Of the ten patients enrolled, eight demonstrated the high mutation rate expected for melanoma, carried expected melanoma-associated mutations (that is, in *BRAF*, *NRAS*, and others) and predominantly C→T transitions (consistent with ultraviolet exposure), and expressed multiple melanoma markers (Extended Data Fig. 1a–c). For these 8 patients, 13–20 immunizing long peptides (IMP) per patient (with lengths of 15–30 amino acids) were synthesized and grouped into 4 separate immunizing pools (Supplementary Information 5). Six patients initiated vaccination (median time of 18 weeks from surgery to vaccine administration) and each completed the full series of five priming and two booster vaccinations. Treatment-related adverse events consisted of mild flu-like symptoms, injection site reactions, rash, and fatigue (Supplementary Information 4b).

At a median follow-up of 25 months (range 20–32) after vaccination, four patients who entered the study with stage IIIB/C disease remained without disease recurrence. Two patients entered with previously untreated stage IVM1b disease (lung metastases); both had disease recurrence evident on restaging scans obtained after the last vaccination. Subsequently, both patients underwent treatment with the anti-PD-1 antibody pembrolizumab and, after four doses, both achieved complete radiographic responses that are ongoing (note that complete radiographic response rate of pembrolizumab as first-line treatment for metastatic melanoma was reported as 6.1% (ref. 5)) (Fig. 1b and Extended Data Fig. 1d).

Overlapping 15- to 16-mer assay peptides (ASP) spanning the entirety of each IMP and 9- to 10-mer peptides corresponding to each predicted class I epitope (EPT) were prepared and pooled to match the corresponding IMP pool (Fig. 2a). When monitored by *ex vivo* interferon (IFN)- γ enzyme-linked immunospot (ELISPOT) assay, peripheral blood mononuclear cells (PBMCs) reactivity was observed to a median of three of four pools of overlapping ASP ($P < 0.005$), suggesting the generation of potent responses against multiple predicted epitopes for all six patients (Fig. 2b). *Ex vivo* responses to these peptide pools were undetectable before vaccination but were

¹Department of Medical Oncology, Dana-Farber Cancer Institute, Boston, Massachusetts 02215, USA. ²Department of Medicine, Brigham and Women's Hospital, Boston, Massachusetts 02215, USA. ³Harvard Medical School, Boston, Massachusetts 02215, USA. ⁴Broad Institute of MIT and Harvard, Cambridge, Massachusetts 02142, USA. ⁵Department of Cancer Immunology and Virology, Dana-Farber Cancer Institute, Boston, Massachusetts 02215, USA. ⁶Department of Biostatistics and Computational Biology, Dana-Farber Cancer Institute, Boston, Massachusetts 02215, USA. ⁷Center for Virology and Vaccine Research, Beth Israel Deaconess Medical Center, Boston, Massachusetts 02215, USA. ⁸Ragon Institute of MGH, MIT, and Harvard, Cambridge, Massachusetts 02139, USA. ⁹Center for Immuno-Oncology (CIO), Dana-Farber Cancer Institute, Boston, Massachusetts 02215, USA. ¹⁰Department of Pathology, Brigham and Women's Hospital, Boston, Massachusetts 02215, USA. ¹¹CuriRx, Inc., Wilmington, Massachusetts 01887, USA. ¹²Oncovir, Inc., 3203 Cleveland Avenue, NW, Washington DC 20008, USA. ¹³Department of Surgery, Brigham and Women's Hospital, Boston, Massachusetts 02215, USA. ¹⁴Department of Pathology, Massachusetts General Hospital, Boston Massachusetts 02214, USA. ¹⁵Center for Cancer Research, Massachusetts General Hospital, Boston Massachusetts 02214, USA. †Present address: Neon Therapeutics, Inc. Cambridge, Massachusetts 02139, USA.

*These authors contributed equally to this work.

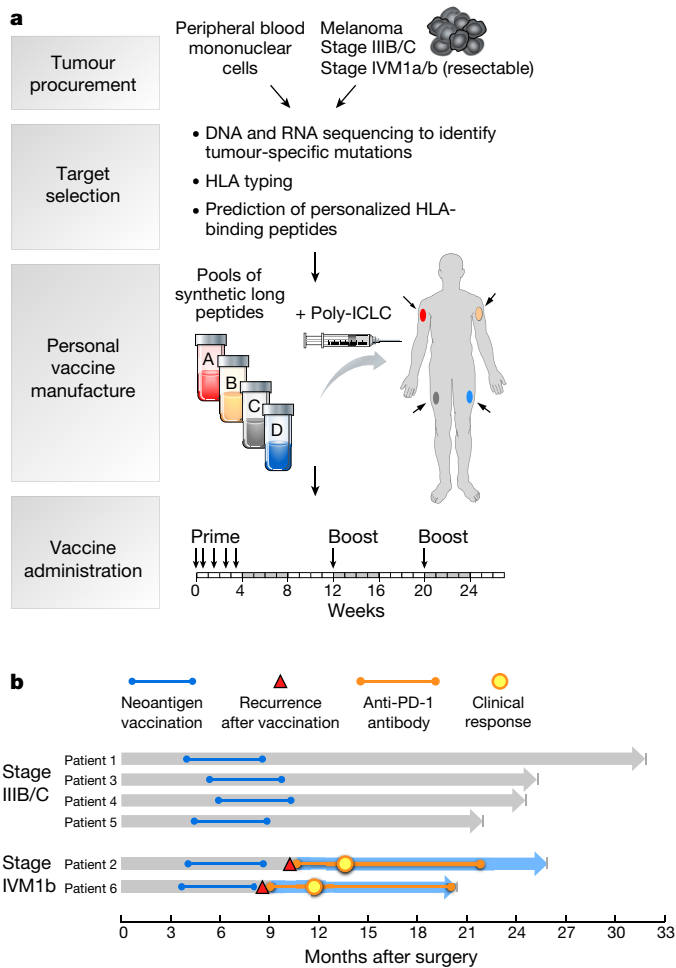


Figure 1 | Generation of a personal, multi-peptide neoantigen vaccine for patients with high-risk melanoma. **a**, Somatic mutations were identified by WES of melanoma and germline DNA and their expression confirmed by tumour RNA-seq. Immunizing peptides were selected on the basis of HLA binding predictions (Methods). Each patient received up to 20 long peptides in four pools. **b**, Clinical event timeline for six vaccinated patients from surgery until time of data cutoff (36 months from study initiation).

already evident at the time of earliest sampling, and were sustained over time. By intracellular cytokine staining (ICS), most *ex vivo* IFN- γ -positive PBMC responses against peptide pools were generated by CD4⁺ T cells (Fig. 2c and Extended Data Fig. 2a). While neoantigen-reactive CD8⁺ T-cell responses were not observed by IFN- γ ELISPOT or ICS directly *ex vivo*, 8 out of 17 (47%) pools of EPT across the six patients (at least one EPT pool per patient) stimulated detectable IFN- γ secretion after a single round of *in vitro* expansion ('pre-stimulation') with the peptides (Fig. 2d and Extended Data Fig. 3a, b). Responses against these EPT pools were absent in pre-stimulated samples collected before vaccination, indicating the generation of new circulating CD8⁺ T-cell responses after vaccination (Extended Data Fig. 3b). For all patients, >30% of neoantigen-reactive CD4⁺ and CD8⁺ T cells were polyfunctional, as evidenced by secretion of two or three inflammatory cytokines (IFN- γ , tumour-necrosis factor (TNF)- α , interleukin (IL)-2) (Extended Data Figs 2b–d and 3c, d).

To identify which predicted epitopes within the peptide pools stimulated the T-cell responses, we deconvoluted all pools by either *ex vivo* or pre-stimulation ELISPOT assays (Extended Data Figs 4a, b and 5). Of 173 9- to 10-mer EPT tested, derived from 91 IMP, CD8⁺ T cells were reactive against EPT from 15 (16%) immunizing peptides (2–4 immunogenic peptides per patient) (Extended Data Fig. 5 and Supplementary Information 5). For CD4⁺ T-cell responses, we tested 297 ASP across 6 patients, corresponding to 97 IMP, and detected

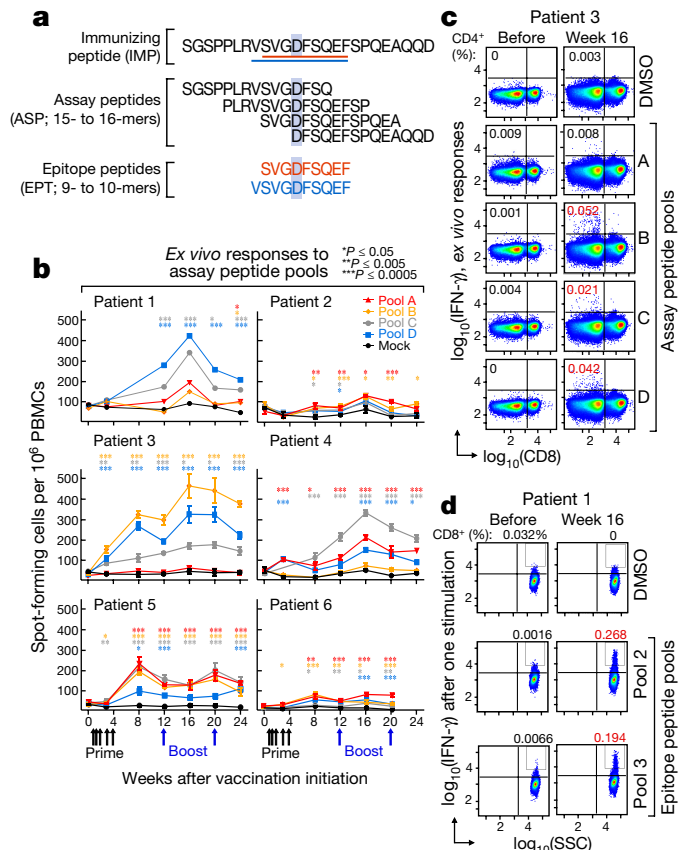


Figure 2 | Vaccination induces strong multi-functional CD4⁺ and CD8⁺ T-cell responses in patients with high-risk melanoma. **a**, Schema of immunizing (IMP), assay (ASP), and epitope (EPT) peptides. Mutated amino acid shaded. **b**, *Ex vivo* IFN- γ ELISPOT of PBMCs, with duplicate or triplicate wells per time point (error bars, s.e.m.; see Methods for statistical analysis). **c**, *Ex vivo* ICS of patient 3 PBMCs before and after vaccination, pre-gated on CD3⁺ T cells. DMSO, dimethylsulfoxide. **d**, Patient 1 CD8⁺ T-cell responses after one round of pre-stimulation with EPT peptide pools, pre-gated on CD8⁺ T cells.

responses against ASP from 19 IMP *ex vivo*, and an additional 39 IMP after one round of pre-stimulation, for a total of 58 (60%) IMP (Extended Data Fig. 5 and Supplementary Information 6).

Thirty-four T-cell lines with reactivity against each of the *ex vivo* CD4⁺-defined and pre-stimulated CD8⁺ targets were evaluated for sensitivity and specificity by incubation with CD4⁺/CD8⁺-depleted PBMC loaded exogenously with mutated or, for single amino-acid changes, wild-type peptides over a range of concentrations. In 24 (86%) out of 28 T-cell lines with reactivity against a mutated peptide, we confirmed preferential reactivity to the mutated compared with the corresponding wild-type peptide (Fig. 3a and Extended Data Fig. 4c). For several predicted epitopes, reactive T-cell populations were observed at peptide concentrations as low as ~10 pM (for example, CD4⁺ T-cell response against mutated *RUSC2* (patient 1); CD8⁺ T-cell response against mutated *COL22A1* (patient 5)), potentially enabling recognition of tumour cells presenting few peptide–MHC complexes⁶. These data demonstrate the high level of specificity for neoantigens over corresponding wild-type antigens. Of the six T-cell lines directed against epitopes predicted to arise from novel open reading frames (neoORFs), several were found highly avid for these epitopes (for example, CD4⁺ T-cell responses against the *CASP5* neoORF (patient 1)). Neoantigen-reactive CD4⁺ (Extended Data Fig. 6a) and CD8⁺ T cells (Fig. 3b) were not detected in samples before vaccination, even after one round of pre-stimulation. Notably, 10% of IMP elicited both CD8⁺ and CD4⁺ T-cell responses.

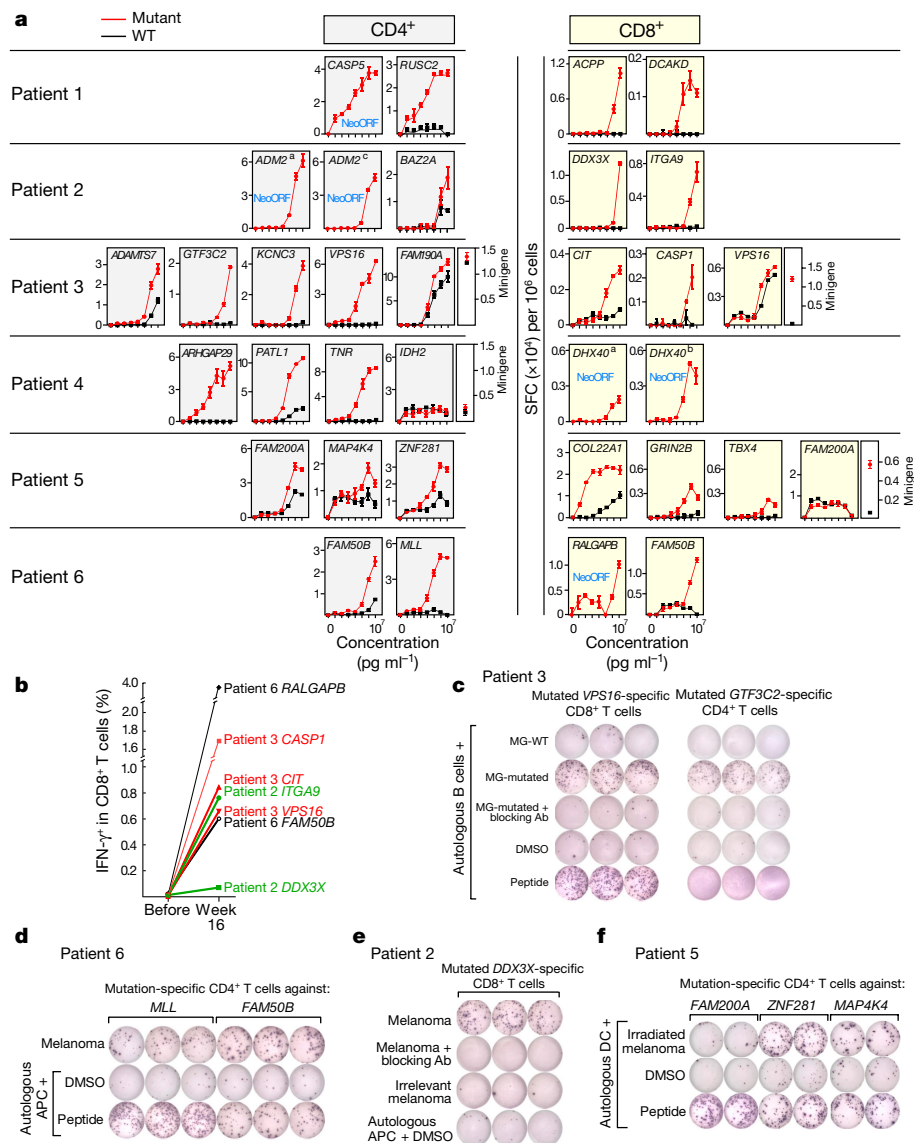


Figure 3 | Vaccine-induced T cells discriminate mutated from wild-type antigens and detect endogenously processed and presented peptides.

a, IFN- γ secretion by neoantigen-reactive T-cell lines against mutated and wild-type peptides at several doses, focusing on neoantigens generating *ex vivo* CD4⁺ and pre-stimulated CD8⁺ T-cell responses (error bars, s.e.m.). **b**, ICS of CD8⁺ T-cell lines stimulated with EPT peptides pre- and post-vaccination. **c**, IFN- γ secretion by patient 3 neoantigen-specific T-cell lines against minigene (MG)-nucleofected B cells, with

We used multiple approaches to confirm that the detected T-cell responses were directed against endogenously processed and presented neoantigens. First, we observed recognition by neoantigen-reactive CD4⁺ (14 out of 19 (73%)) and CD8⁺ (15 out of 15 (100%)) T-cell lines of autologous antigen-presenting cells (APCs) expressing tandem minigenes encoding a series of 25-mer peptides (and hence requiring processing for presentation; Methods) spanning the predicted mutated sites, but not of APCs expressing minigenes encoding corresponding wild-type peptides (Fig. 3c and Extended Data Fig. 6b). Two out of 15 CD8⁺ T-cell lines with clear differential reactivity to mutated versus wild-type peptide-encoding minigenes were unable to discriminate between cells loaded with mutated versus wild-type peptides (Fig. 3a; to *VPS16* (patient 3) and *FAM200A* (patient 5)), suggesting that endogenous processing, but not exogenous loading, differs for the mutated and cognate wild-type peptides. For the CD8⁺ T-cell lines, all mutated minigene responses were uniformly blocked by an anti-HLA class I blocking antibody

or without anti-HLA class I or DR antibodies. **d**, **e**, IFN- γ secretion by patient 6 and patient 2 neoantigen-specific T-cell lines against autologous tumour. **f**, IFN- γ secretion by patient 5 neoantigen-specific CD4⁺ T cells against autologous dendritic cells co-cultured with irradiated autologous melanoma. All T-cell lines originated from week 16 PBMCs; ELISPOT experiments were performed in duplicate or triplicate wells per condition.

(Extended Data Fig. 6b). For the CD4⁺ T-cell lines, 10 out of 19 (52%) were blocked by an anti-HLA-DR blocking antibody; the remainder are presumably restricted by other class II alleles. We observed evidence of cytolytic capacity of these T-cell lines since elevated CD107 $\alpha\beta$ expression was detected after exposure to APCs presenting the mutated minigenes both for CD8⁺ and for CD4⁺ T cells (Extended Data Fig. 6c).

Neoantigen-specific T cells were also tested for reactivity against autologous melanoma cell lines. Flow cytometric analysis of the tumour lines demonstrated variable levels of HLA class I and II expression (Extended Data Fig. 7a). None of the neoantigen-specific T cells recognized cultured tumour cell lines from patients 1, 3, 4, and 5. For patients 2 and 6, we detected recognition of autologous tumour by multiple neoantigen-reactive CD4⁺ and CD8⁺ T cells (Fig. 3d, e). Additionally, CD4⁺ T cells from patient 5 were reactive against autologous dendritic cells exposed to irradiated autologous melanoma cells, demonstrating that tumour-expressed melanoma neoepitopes can be naturally presented by patient APCs (Fig. 3f).

Of note, immunohistochemical evaluation of HLA class I and II expression of the originally surgically resected metastatic tumours, available for five of six patients, demonstrated detectable class I expression in four out of five tumours (patients 2, 4, 5, 6) (Extended Data Fig. 7b, c); thus, these tumours have the potential to be recognized by neoantigen-specific T cells *in vivo*.

To analyse the frequency and phenotype of vaccine-induced CD4⁺ T cells, we generated HLA class II tetramers that detect neoantigen-reactive CD4⁺ T cells. The tetramers detected T cells against *RUSC2* (patient 1) and *ARHGAP29* (patient 4) directly *ex vivo* at week 16, representing approximately 0.03–0.06% of all circulating CD4⁺ T cells, with persistence of *ARHGAP29*-reactive cells at week 24 (Fig. 4a, b, Extended Data Fig. 8c, d and Extended Data Table 2). To characterize the functional state of these cells, we sorted CD4⁺ T cells before vaccination and tetramer-positive CD4⁺ T cells after vaccination in both patients, and compared their gene expression profiles using single-cell RNA-seq. Clustering of T cells showed robust separation of pre- and post-vaccination cells (Fig. 4b and Extended Data Fig. 8d), with hundreds of genes changing their expression after vaccination. These major shifts in gene expression reflected a transition from naive to effector and memory functions, including silencing of genes promoting naive T-cell homeostatic survival (for example, *IL7R* (patient 4)) and fate (for example, *FOXP1* (patient 1)), and upregulation of genes involved in Th1 fate (for example, *TBX21* (patient 4)) and energy metabolism critical for cell proliferation and growth (for example, glucose and glutamine transporters and *MTOR* in patient 4) (Supplementary Information 7). While *SATB1*, a recently described epigenetic repressor of PD-1 (ref. 7), was downregulated in both patients, PD-1 itself was only upregulated in patient 4, suggesting additional mechanisms regulating PD-1.

For patients 2 and 6, who both achieved a complete radiographic response after treatment with pembrolizumab, we tested samples collected after 9–12 months of treatment with pembrolizumab for reactivity against ASP and EPT by IFN- γ ELISPOT. Indeed, CD4⁺ T-cell responses against 25 out of 49 ASP (with 4 novel responses) and CD8⁺ T-cell responses against 2 out of 18 EPT for patient 2 were detected (Fig. 4c and Extended Data Fig. 8a). Similarly, for patient 6, CD4⁺ T-cell responses were detected against 15 out of 61 ASP (with 2 novel responses) and CD8⁺ T-cell responses against 4 out of 32 EPT (with 2 novel responses). Thus, we observed persistence of the vaccine-induced neoantigen responses over time and broadening of the repertoire of neoantigen-specific T cells after checkpoint blockade therapy.

Our study provides proof-of-principle that a personal vaccine can be produced and administered to a patient to generate highly specific immune responses against that individual's tumour. Given the importance of both CD8⁺ and CD4⁺ T cells in mediating tumour cell killing^{8,9}, we used long peptides in the vaccine, leading to activation of both CD8⁺ and CD4⁺ T cells against a substantial proportion of IMP (summarized in Extended Data Fig. 8b). Notably, 20% of IMP induced *ex vivo* CD4⁺ T-cell responses, comparable to the magnitude of responses seen for viral E6 and E7 long peptide therapeutic vaccines in patients with vulvar intraepithelial neoplasia³. Importantly, the proportion of tumour neoantigens inducing a T-cell response after vaccination was substantially higher than the rates (~1% *ex vivo* for CD8⁺ or CD4⁺ T cells) observed in patients who responded clinically to non-antigen-directed immunotherapy, such as checkpoint blockade or tumour-infiltrating lymphocyte therapy^{10–13}. Thus, in agreement with a reported melanoma study showing T-cell responses to a dendritic-cell-based neoantigen vaccine¹⁴, our results demonstrate that a personal neoantigen vaccine broadens the repertoire of neoantigen-specific T cells substantially beyond what is induced by existing immunotherapeutics.

Despite the selection of neoantigens on the basis of predicted presentation by HLA class I, the proportion of neoantigens stimulating class II responses was higher than for class I responses (~60% versus 20%). Nevertheless, this outcome is consistent with recent reports in

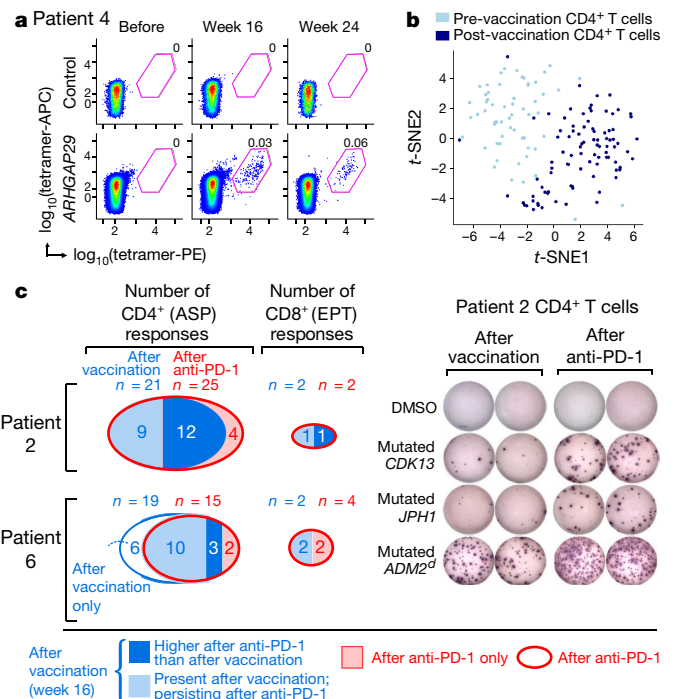


Figure 4 | Vaccine-induced T cells demonstrate broad shifts in their transcriptional programs; the repertoire of neoantigen-specific T cells persists and broadens after PD-1 blockade. **a**, *Ex vivo* class II tetramer staining of patient 4 CD4⁺ T cells. **b**, Visualization of transcriptomes of single CD4⁺ T cells before vaccination and tetramer-positive CD4⁺ T cells after vaccination by *t*-distributed stochastic neighbour embedding (*t*-SNE). **c**, Summary of neoantigen-specific T-cell responses after vaccination and after PD-1 blockade for patients 2 and 6. Example of IFN- γ ELISPOT results are shown for CD4⁺ T cells specific for mutated *CDK13*, *JPH1*, and *ADM2^d* at week 16 after vaccination and after PD-1 blockade for patient 2. For complete response kinetics, see Extended Data Fig. 8a.

mouse models of cancer demonstrating predominantly CD4⁺ T-cell responses upon vaccination with neoepitopes predicted by class I binding algorithms^{15,16}. A combination of structural (precise amino and carboxy termini for class I epitopes versus promiscuous binding properties of peptides to MHC class II proteins^{17–19}), cellular (scarcity of CLEC9A⁺ dendritic cells that may be needed to process long peptides for cross-presentation to CD8⁺ T cells²⁰), and other factors probably explain the predominance of CD4⁺ T-cell responses. Recent studies have highlighted a role for neoantigen-specific CD4⁺ T-cell responses in direct tumour clearance^{8,9,15}. In addition to the licensing of dendritic cells and the activation and maintenance of a tumour-directed CD8⁺ T-cell response²¹, CD4⁺ T cells can exert direct anti-tumour effects independently of CD8⁺ T cells^{21–23}.

In conclusion, we demonstrate that a personal neoantigen vaccine is safe, feasible, and capable of eliciting strong T-cell responses in a clinical setting unconfounded by previous or intercurrent therapy. The use of a personal neoantigen vaccine is anticipated to help address two major challenges for effective cancer immunotherapy: targeting highly heterogeneous tumours and selectively targeting tumour relative to healthy tissues. On the basis of the observed induction of *de novo* T-cell clones that detect multiple individual-specific neoantigens and recognize endogenously processed antigens and autologous tumour cells, our vaccine is likely to target a diversity of malignant clones per patient, thus addressing tumour heterogeneity as well as minimizing the chance of tumour escape by loss of antigen. Future neoantigen vaccine trials will take advantage of improved methods for predicting antigen presentation to increase the fraction of neoantigens inducing tumour-reactive T cells²⁴ and will test for synergy with checkpoint blockade and other immunotherapeutics.

Online Content Methods, along with any additional Extended Data display items and Source Data, are available in the online version of the paper; references unique to these sections appear only in the online paper.

Received 16 February; accepted 16 May 2017.

Published online 5 July 2017.

- Schumacher, T. N. & Schreiber, R. D. Neoantigens in cancer immunotherapy. *Science* **348**, 69–74 (2015).
- Hacohen, N., Fritsch, E. F., Carter, T. A., Lander, E. S. & Wu, C. J. Getting personal with neoantigen-based therapeutic cancer vaccines. *Cancer Immunol. Res.* **1**, 11–15 (2013).
- Kenter, G. G. *et al.* Vaccination against HPV-16 oncoproteins for vulvar intraepithelial neoplasia. *N. Engl. J. Med.* **361**, 1838–1847 (2009).
- Caskey, M. *et al.* Synthetic double-stranded RNA induces innate immune responses similar to a live viral vaccine in humans. *J. Exp. Med.* **208**, 2357–2366 (2011).
- Robert, C. *et al.* Pembrolizumab versus ipilimumab in advanced melanoma. *N. Engl. J. Med.* **372**, 2521–2532 (2015).
- Sykulev, Y., Joo, M., Vturina, I., Tsomides, T. J. & Eisen, H. N. Evidence that a single peptide-MHC complex on a target cell can elicit a cytolytic T cell response. *Immunity* **4**, 565–571 (1996).
- Stephen, T. L. *et al.* SATB1 expression governs epigenetic repression of PD-1 in tumor-reactive T cells. *Immunity* **46**, 51–64 (2017).
- Tran, E. *et al.* Cancer immunotherapy based on mutation-specific CD4⁺ T cells in a patient with epithelial cancer. *Science* **344**, 641–645 (2014).
- Schumacher, T. *et al.* A vaccine targeting mutant IDH1 induces antitumour immunity. *Nature* **512**, 324–327 (2014).
- van Rooij, N. *et al.* Tumor exome analysis reveals neoantigen-specific T-cell reactivity in an ipilimumab-responsive melanoma. *J. Clin. Oncol.* **31**, e439–e442 (2013).
- Rizvi, N. A. *et al.* Mutational landscape determines sensitivity to PD-1 blockade in non-small cell lung cancer. *Science* **348**, 124–128 (2015).
- Linnemann, C. *et al.* High-throughput epitope discovery reveals frequent recognition of neo-antigens by CD4⁺ T cells in human melanoma. *Nat. Med.* **21**, 81–85 (2015).
- Prickett, T. D. *et al.* Durable complete response from metastatic melanoma after transfer of autologous T cells recognizing 10 mutated tumor antigens. *Cancer Immunol. Res.* **4**, 669–678 (2016).
- Carreno, B. M. *et al.* A dendritic cell vaccine increases the breadth and diversity of melanoma neoantigen-specific T cells. *Science* **348**, 803–808 (2015).
- Kreiter, S. *et al.* Mutant MHC class II epitopes drive therapeutic immune responses to cancer. *Nature* **520**, 692–696 (2015).
- Martin, S. D. *et al.* Low mutation burden in ovarian cancer may limit the utility of neoantigen-targeted vaccines. *PLoS ONE* **11**, e0155189 (2016).
- Stern, L. J. *et al.* Crystal structure of the human class II MHC protein HLA-DR1 complexed with an influenza virus peptide. *Nature* **368**, 215–221 (1994).
- Rossjohn, J. *et al.* T cell antigen receptor recognition of antigen-presenting molecules. *Annu. Rev. Immunol.* **33**, 169–200 (2015).
- Falk, K., Rötzschke, O., Stevanović, S., Jung, G. & Rammensee, H. G. Allele-specific motifs revealed by sequencing of self-peptides eluted from MHC molecules. *Nature* **351**, 290–296 (1991).
- Mildner, A. & Jung, S. Development and function of dendritic cell subsets. *Immunity* **40**, 642–656 (2014).

- Spitzer, M. H. *et al.* Systemic immunity is required for effective cancer immunotherapy. *Cell* **168**, 487–502 (2017).
- Haabeth, O. A. *et al.* Idiotype-specific CD4⁺ T cells eradicate disseminated myeloma. *Leukemia* **30**, 1216–1220 (2016).
- Hirschhorn-Cymerman, D. *et al.* Induction of tumoricidal function in CD4⁺ T cells is associated with concomitant memory and terminally differentiated phenotype. *J. Exp. Med.* **209**, 2113–2126 (2012).
- Abelin, J. G. *et al.* Mass spectrometry profiling of HLA-associated peptidomes in mono-allelic cells enables more accurate epitope prediction. *Immunity* **46**, 315–326 (2017).

Supplementary Information is available in the online version of the paper.

Acknowledgements We thank J. Russell and the Dana-Farber Cancer Institute (DFCI) Center for Immuno-Oncology (CIO) staff; M. Copersino (Regulatory Affairs), B. Meyers, C. Harvey, and S. Bartel (Clinical Pharmacy); A. Lako (CIO), M. Bowden (Center for Molecular Oncologic Pathology); O. Sturtevant, H. Negre, S. Y. Kim, M. A. Kelley (Cell Manipulation Core Facility) and the Pasquarello Tissue Bank (all at DFCI); T. Bowman (DFHCC Specialized Histopathology Core Laboratory); the Broad Institute's Biological Samples, Genetic Analysis, and Genome Sequencing Platforms; S. Hodi, G. Dranoff, M. Rajasagi, U. Burkhardt, S. Sarkizova, J. Fan, and P. Bachireddy for discussions; J. Petricciani and M. Krane for regulatory advice; B. McDonough (CSBio) and S. Thorne (CuriRx) for peptide development. This research was made possible by a gift from the Blavatnik Family Foundation, and was supported by grants from the Broad Institute SPARC program and the National Institutes of Health (NCI-1R01CA155010-02 (to C.J.W.), NHLBI-5R01HL103532-03 (to C.J.W.), NCI-SP0RE-2P50CA101942-11A1 (to D.B.K.); NCI-R50 RCA211482A (to S.S.)), from the Francis and Adele Kittredge Family Immuno-Oncology and Melanoma Research Fund (to P.A.O.), the Faircloth Family Research Fund (to P.A.O.), and the DFCI Center for Cancer Immunotherapy Research fellowship (to Z.H.). C.J.W. is a scholar of the Leukemia and Lymphoma Society.

Author Contributions P.A.O. was the principal investigator and Investigational New Drug holder. C.J.W., N.H., P.A.O., and E.F.F. directed the overall study design. Z.H. designed and performed experimental and data analysis with D.B.K., D.J.B., W.Z., L.P., C.C., S.L., and D.J.L.; S.A.S., T.A.C., J.S., J.S., W.J.L., and E.F.F. analysed sequencing data and selected neoantigen targets; D.H.B. and M.S. enabled sample collection and immune monitoring; H.D. and J.R. directed vaccine preparation; A.L. and K.W. designed and generated tetramers; A.G.H. and D.N. designed and performed statistical analyses; T.E., A.M.S., I.J., and K.N. helped design the vaccine formulation; O.O. coordinated clinical research; P.A.O., E.I.B., and C.H.Y. provided patient samples; J.C.A., E.G., and S.J.R. performed pathology review; M.H., N.L., S.G., and G.G. helped devise the computational pipeline; N.H., C.J.W., E.F.F., T.A.C., and E.S.L. developed the overall program strategy. P.A.O., Z.H., E.F.F., N.H., and C.J.W. wrote the manuscript; all authors discussed and interpreted results.

Author Information Reprints and permissions information is available at www.nature.com/reprints. The authors declare competing financial interests: details are available in the online version of the paper. Publisher's note: Springer Nature remains neutral with regard to jurisdictional claims in published maps and institutional affiliations. Readers are welcome to comment on the online version of the paper. Correspondence and requests for materials should be addressed to C.J.W. (cwu@partners.org).

METHODS

No statistical methods were used to predetermine sample size. The experiments were not randomized. The investigators were not blinded to allocation during experiments and outcome assessment.

Study design. Patients with high-risk melanoma provided informed consent and were enrolled between April 2014 and October 2015 to a single centre, phase I clinical trial approved by the Dana-Farber/Harvard Cancer Center Institutional Review Board (NCT01970358). This study was conducted in accordance with the Declaration of Helsinki. Key eligibility criteria were clinically or radiographically evident, pathologically confirmed stage IIIB/C and IVM1a/b melanoma deemed amenable to complete surgical resection and an Eastern Cooperative Oncology Group (ECOG) performance status of 0 or 1. Other requirements included an absolute lymphocyte count of ≥ 800 cells per microlitre, absolute neutrophil count of $\geq 1,500$ cells per microlitre, haemoglobin ≥ 10 g dl⁻¹, platelet count $\geq 100,000$ cells per microlitre, aminotransferases ≤ 2 times the upper limit of the normal range, total serum bilirubin ≤ 1 times the upper limit of the normal range, and serum creatinine ≤ 1.5 times the upper limit of the normal range. Patients with uveal or mucosal melanoma, previous immune modulating or other cancer-directed therapies (except for IFN- α given as systemic adjuvant therapy for a previous melanoma or melanoma recurrence), active autoimmune disease, or an immunosuppressive condition were excluded.

The primary endpoints of the study were safety and feasibility; secondary endpoints were induction of tumour- and neoantigen-specific cellular immune responses and the number of patients alive at 2 years after melanoma resection. A personal neoantigen-targeting vaccine consisting of long peptides combined into four distinct immunizing peptide pools with 0.3 mg of each peptide admixed with 0.5 mg poly-ICLC per pool in a volume of 1 ml was generated as described below, and was administered subcutaneously on days 1, 4, 8, 15, and 22 (priming phase) and weeks 12 and 20 (booster phase). Each of the four neoantigen vaccine pools per patient was assigned to one of four 'non-rotating' extremities (or the left or right midriff as alternative anatomical locations) for each injection.

Clinical assessments. The safety of study treatment was assessed on the basis of the occurrence of adverse events, which were categorized and graded according to National Cancer Institute Common Terminology Criteria for Adverse Events (version 4.0). During the treatment phase, safety assessments were performed on the day of vaccination and 1 week after each vaccination. During the follow-up phase, safety assessments were conducted every 3 months. Surveillance scans (computer tomography or combined position emission tomography/computer tomography) were performed every 6 months; standard RECIST 1.1 criteria were used for assessment of disease recurrence.

Patient samples. Heparinized blood and serum samples were obtained from study participants on Institutional Review Board-approved protocols at the DFCI. Patient PBMCs were isolated by Ficoll/Hypaque density-gradient centrifugation (GE Healthcare) and cryopreserved with 10% DMSO in FBS (Sigma-Aldrich). Cells and serum from patients were stored in vapour-phase liquid nitrogen until the time of analysis. HLA class I and class II molecular typings were determined by PCR-rSSO (reverse sequence specific oligonucleotide probe), with ambiguities resolved by PCR-SSP (sequence specific primer) techniques (One Lambda).

Tumour samples from patients were obtained immediately after surgery. A portion of the sample was removed for formalin fixation and paraffin embedding (FFPE). The remainder of the tissue was carefully minced manually, suspended in a solution of collagenase D (200 U ml⁻¹) and DNase I (20 U ml⁻¹) (Roche Life Sciences), transferred to a sealable plastic bag, and incubated with regular agitation in a Seward Stomacher Laboratory Blender for 30–60 min. After digestion, any remaining clumps were removed and the single-cell suspension was recovered, washed, and immediately frozen in aliquots and stored in vapour-phase liquid nitrogen. For patients 1, 2, 3, 5, 7, 9, and 10, the frozen tumour cell suspensions were used for WES and RNA-seq. For patients 4, 6, 8, and 10 WES and RNA-seq were performed on scrolls from the FFPE tissue (Supplementary Information 1a, b).

Generation of personal neoantigen vaccines. WES. Clinical Laboratory Improvement Amendments (CLIA)-certified WES was conducted by the Clinical Research Sequencing Platform, Broad Institute; CLIA 22D2055652. Library construction from surgical melanoma specimens and matched germline DNA of all ten patients was performed as previously described²⁵. Genomic DNA was sheared, end repaired, ligated with barcoded Illumina sequencing adapters, amplified, and size selected. For patients 1, 2, 3, 4, 7, and 9, whole-exome capture was performed using an Agilent SureSelect Human All Exon 44 Mb version 2.0 bait set (Agilent Technologies)²⁶. For patients 5, 6, 8, and 10, WES was performed using an Illumina Nextera Rapid Capture Exome version 1.2 bait set. The Illumina exome specifically targets approximately 37.7 Mb of mainly exonic regions made up of all targets from the Agilent exome design (Agilent SureSelect All Exon V2), all coding regions of Gencode V11 genes, and all coding regions of RefSeq gene and KnownGene tracks from the UCSC genome browser (<http://genome.ucsc.edu>). Resulting

libraries were then qPCR quantified, pooled, and sequenced with 76 base-paired-end reads using HiSeq 2000 or 2500 sequencers (Illumina). Pooled libraries were normalized to 2 nM and denatured using 0.2 N NaOH before sequencing. Data were analysed using the Broad Picard Pipeline, which includes de-multiplexing, duplicate marking, and data aggregation.

RNA-seq. For RNA-seq library construction, RNA was extracted from frozen cell suspensions (patients 1, 2, 3, 7, 9, 10) or FFPE samples (patients 4, 5, 6, 8, 10) using a Qiagen RNeasy Mini Kit or Qiagen FFPE RNeasy Kit, respectively. RNA-seq libraries were prepared using an Illumina TruSeq Stranded mRNA Library Prep Kit (for cell suspensions) or Illumina's TruSeq RNA Access Library Prep Kit (for FFPE samples). Total RNA was quantified using a Quant-iT RiboGreen RNA Assay Kit and normalized to 5 ng μ l⁻¹. For patients 1, 2, 3, 7, and 9, each sample was transferred into library preparation which was an automated variant of the Illumina TruSeq Stranded mRNA Sample Preparation Kit. This method preserved strand orientation of the RNA transcript. It used oligonucleotide dT beads to select messenger RNA (mRNA) from the total RNA sample. It was followed by heat fragmentation and complementary DNA (cDNA) synthesis from the RNA template. The resultant 500 bp cDNA then went through library preparation (end repair, base 'A' addition, adaptor ligation, and enrichment) using Broad-designed indexed adapters substituted in for multiplexing. For patient 4, the mRNA enrichment step was omitted before library preparation. The resulting libraries were quantified with qPCR using a KAPA Library Quantification Kit for Illumina Sequencing Platforms and then pooled equimolarly. For Illumina sequencing, pooled libraries were normalized to 2 nM and denatured using 0.1 N NaOH before sequencing. Flowcell cluster amplification and sequencing were performed according to the manufacturer's protocols using either a HiSeq 2000 or HiSeq 2500. Each run was a 101 bp paired-end with an eight-base index barcode read. Data were analysed using the Broad Picard Pipeline, which includes de-multiplexing and data aggregation.

For patients 5, 6, 8, and 10, a RNA transcriptome capture method was used. Using Illumina's TruSeq RNA Access Library Prep Kit, a stranded cDNA library was prepared from isolated RNA which was then hybridized to a set of DNA oligonucleotide probes to enrich the library for mRNA transcript fragments. The transcriptome capture targeted 21,415 genes, representing 98.3% of the RefSeq exome (and was the same bait set as the Rapid Capture Exome). Flowcell cluster amplification and sequencing were performed according to the manufacturer's protocols using either a HiSeq 2000 or HiSeq 2500. Each run was a 76 bp paired-end with an eight-base index barcode read. Data were analysed using the Broad Picard Pipeline which includes de-multiplexing and data aggregation.

DNA quality control. Standard Broad Institute protocols as previously described^{27,28} were used for DNA quality control. The identities of all tumour and normal DNA samples were confirmed by mass spectrometric fingerprint genotyping of 95 common single nucleotide polymorphisms by Fluidigm Genotyping (Fluidigm). Sample contamination from foreign DNA was assessed using ContEst²⁹.

Somatic mutation calling. Analyses of WES data of tumour and matched PBMCs (as source of normal germline DNA) from the patients were used to identify the specific coding-sequence mutations, including single-, di-, or trinucleotide variants leading to single amino-acid missense mutations and small insertions/deletions. Output from Illumina software was processed by the 'Picard' data processing pipeline to yield BAM files containing aligned reads (bwa version 0.5.9, to the NCBI Human Reference Genome Build hg19) with well-calibrated quality scores^{27,30}. Somatic alterations were identified using a set of tools within the 'Firehose' pipeline (<http://www.broadinstitute.org/cancer/cga>). Somatic single nucleotide variations were detected using MuTect (Firehose version 13112); somatic small insertions and deletions were detected using Indelocator²⁷ and Strelka³¹. All indels were manually reviewed in Integrative Genomics Viewer³². All somatic mutations, insertions, and deletions were annotated using Oncotator³³. The ABSOLUTE algorithm (version 1.1) was used to calculate the purity and ploidy of the samples. RNA-seq data were processed using PRADA software³⁴. Comparisons of gene expression were conducted against data from GTEx (Analysis V6, dbGaP accession number phs000424.v6.p1, doi:10.1038/ng.2653) and The Cancer Genome Atlas (TCGA) (Broad Institute TCGA Genome Data Analysis Center (2016): Firehose stddata_2016_01_28 run. Broad Institute of MIT and Harvard. doi:10.7908/C11G0KM9).

Identification of target epitopes for peptide design. NetMHCpan version 2.4 was used to identify patient-specific mutation-containing epitopes that were predicted to bind to the MHC class I molecules^{19,35,36}. Thirty peptides of 15–30 amino acids in length ('long peptides') from up to 30 independent mutations were selected and prioritized for peptide preparation. Epitopes were chosen for inclusion on the basis of a pre-defined set of criteria in the following rank order: (1) neoORFs which included predicted binding epitopes; (2) high predicted affinity (<150 nM) somatic single nucleotide variations due to anchor residue changes; (3) high-affinity (<150 nM) somatic single nucleotide variations due to mutations in positions other

than anchor residues; (4) neoORFs with no predicted binding epitopes; (5) lower affinity (<150–500 nM) versions of (2) and (3).

Mutations in oncogenes were given highest priority within each ranked group; otherwise epitopes were ranked by predicted mutated peptide affinity. Only somatic single nucleotide variations that demonstrated expression of the mutated allele were used. Additionally, a variety of possible biochemical properties (hydrophobicity, presence of multiple cysteines) that may have affected the synthesizability or solubility of the long peptide were considered.

Synthesis of long peptides, pooling, and final vaccine preparation. GMP peptides were synthesized and purified (CS Bio) using standard solid-phase synthetic peptide chemistry and reverse-phase high performance liquid chromatography (RP-HPLC). Up to 20 peptides were formulated in an aqueous solution containing $\leq 4\%$ DMSO in isotonic dextrose and mixed into a maximum of four pools (three to five peptides per pool, with a final dose of 0.3 mg of each peptide per vaccine). On the day of vaccine administration, each peptide pool was admixed with 0.5 mg poly-ICLC (Hiltonol; Oncovir) by syringe-to-syringe transfer at the DFCl Clinical Pharmacy.

Melanoma cell-line generation. Fresh tumour-cell suspensions or thawed cryopreserved cells were washed and cultured in tissue culture plates containing OptiMEM GlutaMax media (Gibco, ThermoFisher) supplemented with fetal bovine serum (5%), sodium pyruvate (1 mM), penicillin and streptomycin (100 U ml^{-1}), gentamycin ($50 \mu\text{g ml}^{-1}$), insulin ($5 \mu\text{g ml}^{-1}$), and epidermal growth factor (5 ng ml^{-1} ; Sigma-Aldrich). Cell cultures were dissociated and passaged using versene (Gibco, ThermoFisher). The expanding cell lines were tested mycoplasma free and verified as melanoma through immunohistochemical stains using antibodies against the melanoma markers HMB45, MITF, MART-1, Melan-A, and S100 that were performed in the Dana-Farber/Harvard Cancer Center Specialized Histopathology Core Laboratory.

Immunohistochemical evaluation of primary melanoma cells. Dual immunohistochemical staining of the antigen presentation components: HLA class I (Abcam, EMR8-5, 1:6,000) and HLA class II (Dako, CR3/43 M0775, 1:750) with the melanoma marker SOX10 (EP 268, Cell Marque, 1:1,500) was performed using an automated staining system (Bond III, Leica Biosystems) according to the manufacturer's protocol, as previously described³⁷. Semi-quantitative scoring was performed for the intensity of positive staining of melanoma cell membranes for the marker of interest (0, negative; 1, weak; 2, moderate; 3, strong) and for the percentage of positive staining malignant cells (0–100%). A cumulative 'H score' was obtained by multiplying intensity score (0–3) by the percentage of malignant cells with positive staining (0–100%; with any intensity of positive staining). Stained slides were first reviewed and scored independently by two individuals and subsequently reviewed together with a final, consensus score tabulated as previously described³⁷.

Generation and detection of patient neoantigen-specific T cells. PBMCs were cultured in RPMI-1640 medium supplemented with L-glutamine, non-essential amino acids, HEPES, β -mercaptoethanol, sodium pyruvate, penicillin/streptomycin (Gibco), and 10% AB-positive heat-inactivated human serum (Gemini Bioproduct). For *in vitro* expansion ('pre-stimulation') of antigen-specific T cells, PBMCs were stimulated in 24-well cell culture plates at 5×10^6 cells per well with individual ($2 \mu\text{g ml}^{-1}$) or pooled peptides (each at $2 \mu\text{g ml}^{-1}$) in the presence of IL-7 (20 ng ml^{-1} ; R&D Systems). On day 3, low-dose IL-2 (20 U ml^{-1} ; Amgen) was added. Half-medium change and supplementation of cytokines were performed every 3 days, as described previously³⁸. After 10–21 days, T-cell (referred to as 'T-cell lines') specificity was tested against peptide, minigenes, or autologous tumour by interferon (IFN)- γ ELISPOT or CD107 $\alpha\beta$ degranulation assay in RPMI-1640 medium supplemented with penicillin/streptomycin and 10% FBS (complete RPMI). For deconvolution of CD8⁺ T-cell responses, CD8⁺ T cells were enriched with CD8⁺ T-cell Isolation Kit beads (Miltenyi Biotec) before plating for ELISPOT.

Antigen formats for immune monitoring. Assay (ASP) and predicted class I epitope peptides (EPT) were synthesized and lyophilized (from either JPT Peptide Technologies; or RS Synthesis) (>80% purity). ASP were 15–16 amino acids and overlapped by at least 11 amino acids, covering the IMP sequence. EPT were 9–10 amino acids. Peptides for generation of class II tetramers were synthesized to >90% purity (21st Century Biochemicals). Minigenes were constructed³⁹ such that (1) for non-synonymous mutations, they encoded the mutated amino acid and surrounding upstream and downstream native amino acids for a total length of ~25 amino acids; (2) for frame-shift mutations, they encoded the entire corresponding immunizing peptide. Multiple minigenes (3–7 per plasmid) for a given patient were arranged in tandem without additional linker sequences and synthesized as a gBlock (Integrated DNA Technologies). Each tandem minigene construct was inserted into a pcDNA3.1 vector using available EcoRI and BamHI cut sites. RNA was generated by *in vitro* transcription of the tandem minigene plasmids using an mMACHINE Ultra Kit (Thermo Fisher). Twenty micrograms of

the *in vitro* transcription RNA was introduced into autologous positively selected CD19⁺ B cells (CD19 Microbeads, Miltenyi Biotec) by nucleofection using V-buffer and the X-001 program (Amaxa Cell Line Nucleofector Kit V, Lonza). The B cells were used within 24 h of transfection. Transfection efficiency was typically 70–85%, on the basis of 24 h green fluorescent protein (GFP) expression after nucleofection with control *in vitro* transcription RNA generated using a pcDNA3.1-GFP plasmid. Tandem constructs containing the wild-type versions of the minigenes with non-synonymous mutations were also similarly designed.

In some experiments, antigen-specific T cells were tested against autologous melanoma cells. In other experiments, autologous irradiated melanoma cells were co-cultured with autologous dendritic cells. Immunomagnetically isolated CD14⁺ cells (Human CD14 MicroBeads; Miltenyi Biotec) were cultured in complete RPMI containing 120 ng ml^{-1} GM-CSF and 70 ng ml^{-1} IL-4 at 3×10^6 cells per well in a six-well plate. Media were exchanged on days 3 and 5. For feeding of melanoma cells to autologous dendritic cells, melanoma cells were irradiated with 150 Gy and cultured in serum-free RPMI overnight. Dendritic cells were cultured with or without melanoma cells in complete RPMI (0.25×10^6 dendritic cells and 0.25×10^6 melanoma cells) in a 48-well plate for 5 h at 37°C, followed by addition of $30 \mu\text{g ml}^{-1}$ poly-inosinic-poly-cytidylic acid (Sigma-Aldrich) to induce dendritic cell maturation. After overnight culture, dendritic cells were harvested and used as APCs on ELISPOT assays.

IFN- γ ELISPOT assay. IFN- γ ELISPOT assays were performed using 96-well MultiScreen Filter Plates (Millipore), coated with $2 \mu\text{g ml}^{-1}$ anti-human IFN- γ mAb overnight (1-D1K, Mabtech). Plates were washed with PBS and blocked with complete RPMI before use. For pre-stimulated T cells, 5×10^3 T cells and 1×10^4 CD8⁺ T cells for detection of CD4⁺ and CD8⁺ T-cell responses, respectively, were co-cultured with 1×10^4 autologous CD4⁺ and CD8⁺ T-cell-depleted PBMCs, 8×10^4 B cells, 1×10^4 autologous tumour cells, or 5×10^3 autologous dendritic cells, unless otherwise stated (Fig. 3e: 2×10^4 CD8⁺ T cells plated; Fig. 4c: 1×10^4 T cells plated). APCs were pulsed with peptides ($2\text{--}10 \mu\text{g ml}^{-1}$), or peptides were directly added to the ELISPOT wells with APCs and incubated with T cells overnight in complete RPMI at 37°C. For *ex vivo* ELISPOT, 2×10^5 PBMCs were plated with $2 \mu\text{g ml}^{-1}$ peptide and incubated overnight. Plates were rinsed with PBS containing 0.05% Tween-20 and then $1 \mu\text{g ml}^{-1}$ anti-human IFN- γ mAb (7-B6-1-Biotin, Mabtech) was added, followed by Streptavidin-ALP (Mabtech). After rinsing, SIGMA FAST BCIP/NBT (5-bromo-4-chloro-3-indolyl phosphate/nitro blue tetrazolium; Sigma-Aldrich) was used to develop the immunospots, and spots were imaged and enumerated (Cellular Technology Limited). For some experiments, APCs were cultured on the ELISPOT plate with HLA blocking antibodies ($10 \mu\text{g ml}^{-1}$; pan anti-DR (clone: L243) or anti-HLA I (clone: W6/32)) for 1–2 h in advance of the addition of peptides and T cells to the wells. *Ex vivo* responses were scored positive if >55 spot-forming cells were detected and were at least 1.5 s.d. over the DMSO control (>3 s.d. over background for patients 5 and 6). For Fig. 2b, for each patient, the numbers of spot-forming cells were regressed on assay, time, and the interaction of assay and time using repeated-measures models with an unstructured covariance. *P* values (*t*-test) for the comparisons of each pool against the mock were adjusted using the Benjamini–Hochberg procedure to maintain an overall alpha value of 0.05 at each time within each patient.

ICS and CD107 $\alpha\beta$ degranulation assay. For *ex vivo* intracellular cytokine detection, PBMCs were stimulated with $5 \mu\text{g ml}^{-1}$ peptide or 50 ng ml^{-1} PMA (Sigma-Aldrich) and $1 \mu\text{g ml}^{-1}$ ionomycin (Sigma-Aldrich) in complete RPMI with $10 \mu\text{g ml}^{-1}$ brefeldin A (Sigma-Aldrich) at 37°C overnight. For detection of cytokines from pre-stimulated CD8⁺ T cells, 2×10^6 T cells were re-stimulated with 1×10^6 T-cell-depleted PBMCs pulsed with $5 \mu\text{g ml}^{-1}$ peptide in complete RPMI with $10 \mu\text{g ml}^{-1}$ brefeldin A at 37°C overnight. Subsequently, cells were stained with antibodies against surface markers for 20 min at 4°C, followed by fixation with 1% formaldehyde at 4°C for 20 min, and then stained with antibodies against cytokines in 0.5% saponin solution at 4°C for 1 h to overnight. Anti-CD4 antibody (conjugated with PerCP-Cy5.5, clone OKT-4, eBioscience), CD8 (PE-Cy7, SK1, eBioscience), CD3 (APCCy7, HIT3a, Biolegend), CD14 (BV510, M5E2, Biolegend), CD19 (BV510, HIB19, Biolegend), IFN- γ (APC, 4S.B3, Biolegend), TNF- α (BV421, Mab11, Biolegend), and IL-2 (PE, MQ1-17H12, Biolegend) were used. A CD107 $\alpha\beta$ degranulation assay was performed by culturing 5×10^5 T cells and 1.5×10^5 target minigene-expressing B cells with Alexa Fluor 647-conjugated CD107 α (H4A3) and CD107 β (H4B4) antibodies (BD Biosciences) in complete RPMI for 6 h at 37°C. Cells were stained with anti-CD4, -CD8, and -CD69 (Pacific Blue, FN50, Biolegend) antibodies for 30 min at room temperature, followed by fixation with 4% formaldehyde. Flow cytometry analysis was performed on a BD FACSCanto II High Throughput Sampler (HTS) instrument.

Generation of HLA-DR tetramers loaded with defined neoantigen peptides. DR1/CLIP or DR4/CLIP complexes were expressed in stably transfected CHO cells as previously described⁴⁰. The DR α and DR β chain extracellular domains carried Jun and Fos dimerization domains; a C-terminal BirA site was attached

to the DR α chain to enable site-specific biotinylation. The peptide binding site was occupied by a CLIP peptide that was linked through a thrombin-cleavable linker to the N terminus of the mature DR β chain. DR/CLIP complexes were purified from CHO cell supernatants by affinity chromatography using mAb L243 (American Type Culture Collection). Purified DR molecules were biotinylated with a 1:20 molar ratio of BirA:DR as described⁴⁰. Before peptide loading, DR complexes were treated with thrombin for 2 h to release the CLIP peptide. Peptide-exchange reactions were performed with a 15-fold molar excess of dansyl-labelled peptides (21st Century Biochemicals) in a buffer containing 50 mM sodium citrate, 50 mM J10 (ref. 41), 100 mM NaCl, and 1 \times protease inhibitor cocktail overnight at 30 °C. DR/peptide complexes were separated from unbound peptide using a Superose 12 HPLC gel filtration column (Amersham). DR molecules loaded with defined neoantigen peptides were then isolated using an anti-dansyl affinity column. Complexes were eluted from the column using 50 mM CAPS, pH 11.5, and neutralized with 1 M phosphate, pH 6.0. Biotinylated DR/peptide monomers were buffer exchanged with PBS, concentrated to >1 mg ml⁻¹, and frozen in aliquots at -80 °C. Fluorophore-labelled streptavidin (either PE or APC) was added to biotinylated DR/peptide monomers at a 1:4 molar ratio in four separate additions over 60 min at room temperature.

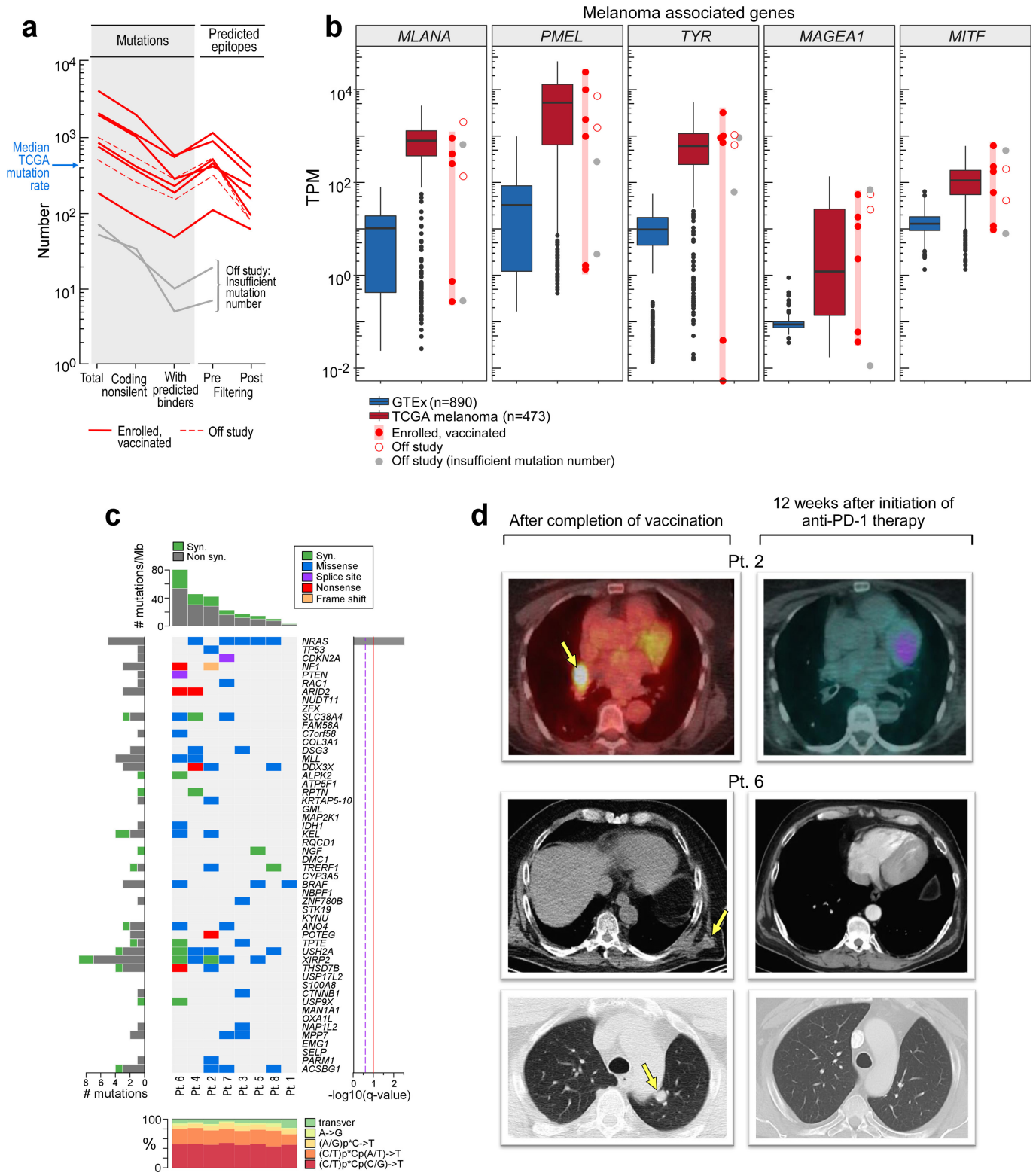
Tetramer labelling of CD4⁺ T cells. Patient PBMCs that were CD4-enriched using a CD4⁺ T-cell Isolation Kit (Miltenyi Biotec) were stained with both APC- and PE-labelled tetramers at 20 μ g ml⁻¹ in RPMI containing 10% FBS, 10 mM HEPES, 2 mM glutamine and 50 U ml⁻¹ penicillin/streptomycin for 1 h at room temperature. DR/CLIP tetramers were used as negative controls. The cell density during staining was 10 \times 10⁶ to 20 \times 10⁶ cells per millilitre. Unbound tetramer was removed using two washes with flow staining buffer (PBS + 2% FBS). Cells were then stained with Live/Dead Aqua (Invitrogen) for 15 min at room temperature, followed by staining with anti-CD4 (Alexa Fluor700, OKT4, Biolegend), anti-CD3 (BV421, UCHT1, Biolegend), and anti-CD14/CD19 (BV510) for 20 min at 4 °C. Cells were washed once with PBS and analysed on a BD Aria cell sorter.

Single-cell transcriptome data generation and analysis. Single-cell transcriptomes of CD4⁺ T cells before vaccination and of class II tetramer-positive CD4⁺ T cells after vaccination were generated using the CEL-Seq2 protocol with the following modifications: single cells were sorted into 0.6 μ l of 1% NP-40 buffer in a 384-well plate, into which 0.6 μ l of barcoded reverse transcriptase reaction primers and a mixture of dNTPs were added. The plate was incubated at 65 °C for 5 min, and then moved immediately to ice. Reverse transcription, the second-strand synthesis reaction, and the *in vitro* transcription reaction were performed as previously described⁴². Amplified RNA was fragmented at 80 °C for 3 min and cleaned up with RNAClean XP beads. Amplified RNA was converted to cDNA using random priming, and then Illumina adaptor sequences were added by PCR. Paired-end sequencing was performed on a HiSeq 2500 in high-output run mode. Raw universal molecular identifier data were first filtered to remove all universal molecular identifiers that had fewer than ten corresponding reads. All cells that had at least 200 genes with non-zero universal molecular identifier counts and < 25% of universal molecular identifiers originating from mitochondrial genes were retained for downstream analysis. All genes that were not detected in at least three cells were excluded. Linear (principal components) and nonlinear (*t*-distributed

stochastic neighbour embedding) dimensionality reduction was performed with the Seurat package⁴³. The SCDE package⁴⁴ was used to identify differentially expressed genes.

Data availability. All data are available from the corresponding author upon reasonable request.

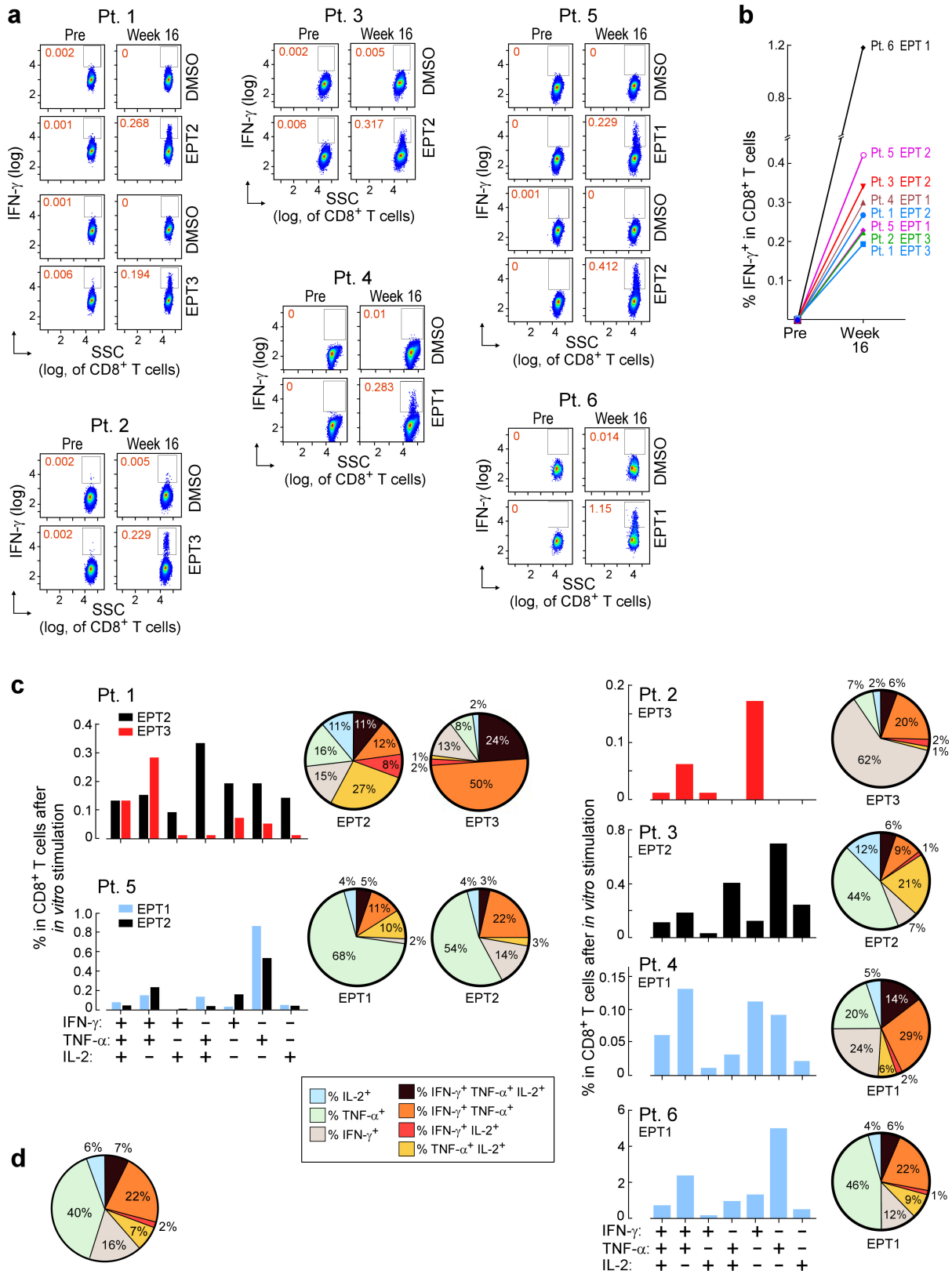
25. Fisher, S. *et al.* A scalable, fully automated process for construction of sequence-ready human exome targeted capture libraries. *Genome Biol.* **12**, R1 (2011).
26. Gnirke, A. *et al.* Solution hybrid selection with ultra-long oligonucleotides for massively parallel targeted sequencing. *Nat. Biotechnol.* **27**, 182–189 (2009).
27. Chapman, M. A. *et al.* Initial genome sequencing and analysis of multiple myeloma. *Nature* **471**, 467–472 (2011).
28. Berger, M. F. *et al.* The genomic complexity of primary human prostate cancer. *Nature* **470**, 214–220 (2011).
29. Cibulskis, K. *et al.* ContEst: estimating cross-contamination of human samples in next-generation sequencing data. *Bioinformatics* **27**, 2601–2602 (2011).
30. DePristo, M. A. *et al.* A framework for variation discovery and genotyping using next-generation DNA sequencing data. *Nat. Genet.* **43**, 491–498 (2011).
31. Saunders, C. T. *et al.* Strelka: accurate somatic small-variant calling from sequenced tumor-normal sample pairs. *Bioinformatics* **28**, 1811–1817 (2012).
32. Robinson, J. T. *et al.* Integrative genomics viewer. *Nat. Biotechnol.* **29**, 24–26 (2011).
33. Ramos, A. H. *et al.* Oncotator: cancer variant annotation tool. *Hum. Mutat.* **36**, E2423–E2429 (2015).
34. Torres-García, W. *et al.* PRADA: pipeline for RNA sequencing data analysis. *Bioinformatics* **30**, 2224–2226 (2014).
35. Hoof, I. *et al.* NetMHCpan, a method for MHC class I binding prediction beyond humans. *Immunogenetics* **61**, 1–13 (2009).
36. Lundegaard, C., Lund, O. & Nielsen, M. Prediction of epitopes using neural network based methods. *J. Immunol. Methods* **374**, 26–34 (2011).
37. Roemer, M. G. *et al.* Classical hodgkin lymphoma with reduced β 2M/MHC Class I expression is associated with inferior outcome independent of 9p24.1 status. *Cancer Immunol. Res.* **4**, 910–916 (2016).
38. Cai, A. *et al.* Mutated BCR-ABL generates immunogenic T-cell epitopes in CML patients. *Clin. Cancer Res.* **18**, 5761–5772 (2012).
39. Lu, Y. C. *et al.* Efficient identification of mutated cancer antigens recognized by T cells associated with durable tumor regressions. *Clinical Cancer Res.* **20**, 3401–3410 (2014).
40. Day, C. L. *et al.* Ex vivo analysis of human memory CD4 T cells specific for hepatitis C virus using MHC class II tetramers. *J. Clin. Invest.* **112**, 831–842 (2003).
41. Call, M. J. *et al.* *In vivo* enhancement of peptide display by MHC class II molecules with small molecule catalysts of peptide exchange. *J. Immunol.* **182**, 6342–6352 (2009).
42. Hashimshony, T. *et al.* CEL-seq2: sensitive highly-multiplexed single-cell RNA-seq. *Genome Biol.* **17**, 77 (2016).
43. Satija, R., Farrell, J. A., Gennert, D., Schier, A. F. & Regev, A. Spatial reconstruction of single-cell gene expression data. *Nat. Biotechnol.* **33**, 495–502 (2015).
44. Kharchenko, P. V., Silberstein, L. & Scadden, D. T. Bayesian approach to single-cell differential expression analysis. *Nat. Methods* **11**, 740–742 (2014).
45. Lundegaard, C. *et al.* NetMHC-3.0: accurate web accessible predictions of human, mouse and monkey MHC class I affinities for peptides of length 8–11. *Nucleic Acids Res.* **36**, W509–12 (2008).



Extended Data Figure 1 | See next page for caption.

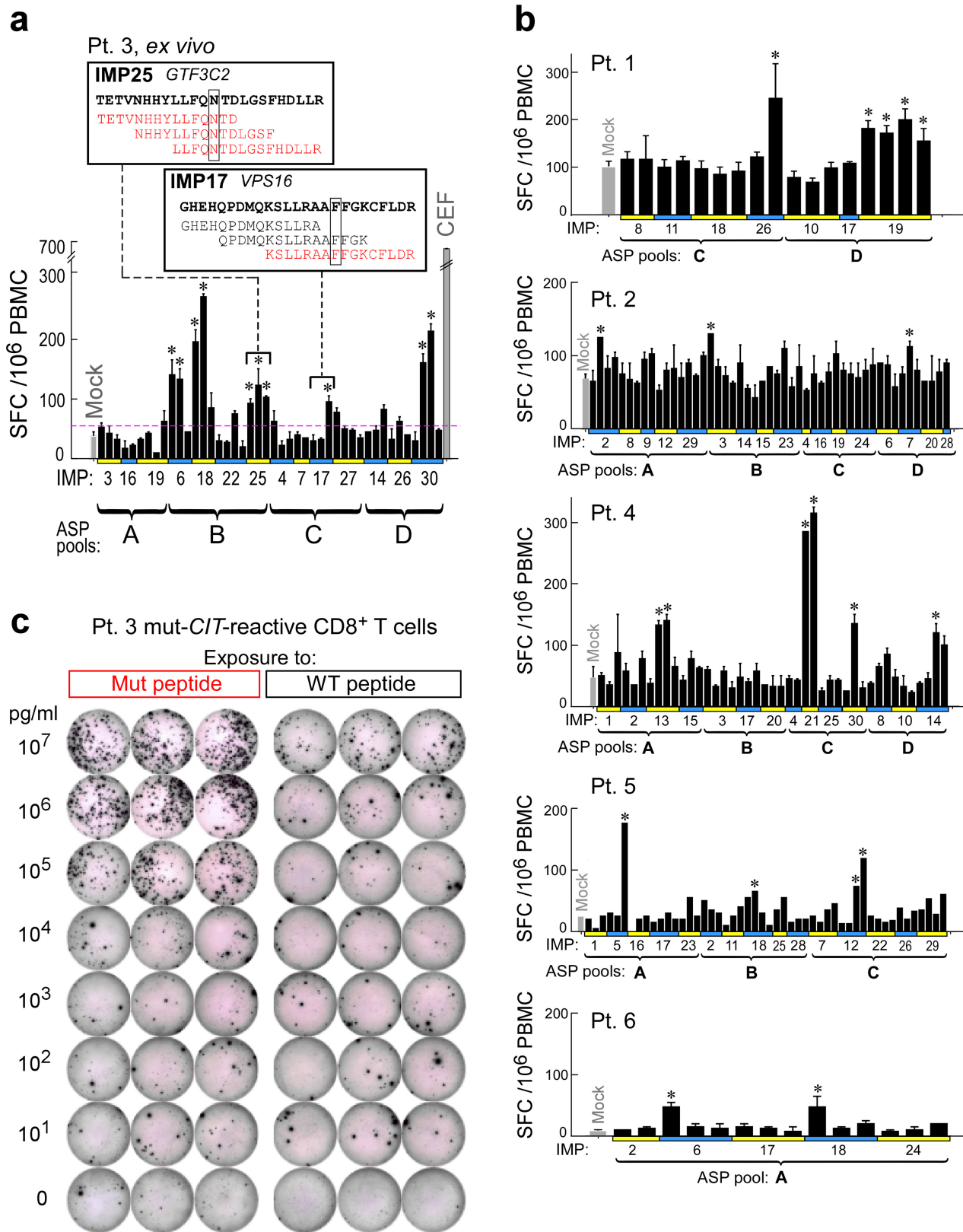
Extended Data Figure 1 | Mutational landscape of patient melanoma and radiographic evidence of complete response after anti-PD-1 therapy for patients 2 and 6. **a**, Numbers of mutations and predicted epitopes per patient tumour. Red solid lines, patients with vaccines generated and vaccinations completed ($n = 6$); red dashed lines, vaccines generated but vaccinations not initiated ($n = 2$); grey, insufficient mutation number for vaccine generation ($n = 2$). **b**, Expression (measured and normalized as transcripts per million base pairs (TPM) from the RNA-seq data) of known melanoma-associated genes in the tumour specimens for all ten patients entered into the trial (circles) compared with skin tissue (blue box, (GTEx data)) and melanoma from TCGA (red box; see Methods for analysis). The upper, middle, and lower hinge of the box are 75%, 50%, and 25% quantiles. All points above or below whiskers are the outliers. **c**, The overall mutational landscape of the eight patient melanoma samples for which immunizing peptides were generated (top, number of mutations per megabase; bottom, distribution of nucleotide changes) and the presence of mutations in genes previously identified as recurrent in melanoma TCGA samples ($n = 290$) by the MutSig2CV algorithm (middle, doi:10.7908/C1J67GCG; genes ordered on the basis of significance of recurrence reported per TCGA, Supplementary Information 2). **d**, Patient (Pt.) 2. Left: positron emission tomography/computed tomography

(PET/CT) scans obtained 8 weeks after the last booster vaccine demonstrate new intensely fludeoxyglucose F 18 (FDG)-avid right hilar lymphadenopathy measuring ~ 2.1 cm (maximal standardized uptake value 20.3 (yellow arrow)). Right: PET/CT obtained 12 weeks later, after four doses of pembrolizumab at 2 mg per kg (body weight) given every 3 weeks, revealing complete interval resolution of the right hilar lymphadenopathy consistent with a complete response. Patient 6. Left panels: CT scans of the chest obtained 1 week after the last booster vaccine demonstrate multiple soft-tissue nodules along the left lateral and posterolateral chest wall (left upper panel, yellow arrow indicates a $2.1 \text{ cm} \times 1.8 \text{ cm}$ soft-tissue nodule as an example) and a left lower lobe pulmonary nodule (left lower panel, yellow arrow). Right panels: CT scans obtained 16.5 weeks later, after four doses of pembrolizumab at 2 mg per kg (body weight) given every 3 weeks, revealing complete interval resolution of all lesions consistent with a complete response. On the upper panels, note that the liver is partly visualized on the pre-treatment scan (left upper panel) as a result of expirational state and not visualized on the post-treatment scan (right upper panel) as a result of inspirational state. The cross sections visualizing the soft-tissue metastases in the left chest wall versus their resolution after treatment correspond.



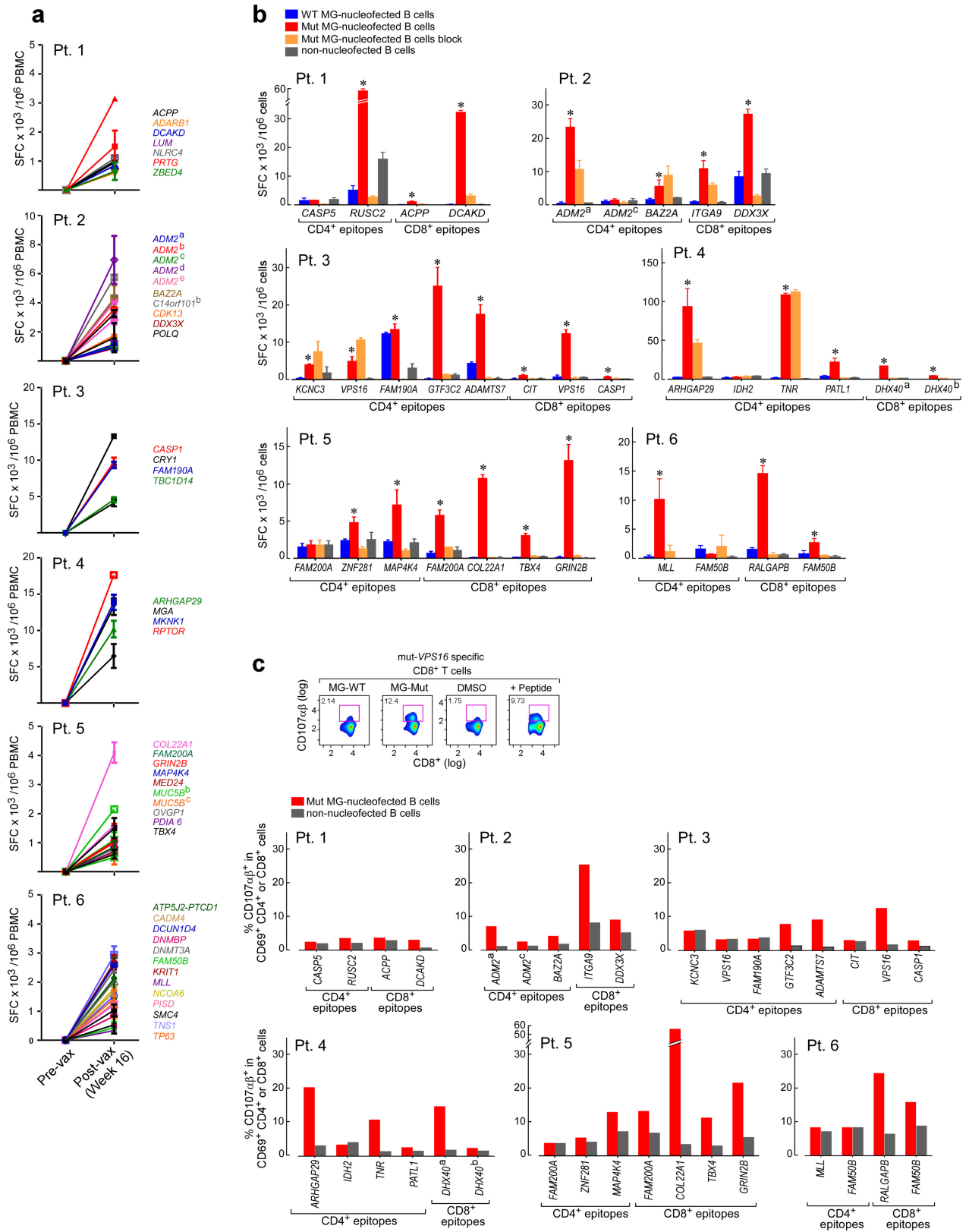
Extended Data Figure 3 | Polyfunctional neoantigen-specific CD8⁺ T-cell responses are induced by vaccination in all six patients. Frequencies of CD8⁺ T cells secreting cytokines in response to pools of 9- to 10-mer predicted class I EPT after a single round of pre-stimulation. PBMCs were cultured with EPT pools for 10–21 days followed by ICS. **a**, IFN- γ -producing CD8⁺ T cells detected by flow cytometry pre-vaccination and at week 16 after vaccination for all six vaccinated patients. FACS plots were pre-gated on CD8⁺ T cells. Percentages shown in red are frequencies of EPT-pool-reactive IFN- γ ⁺ cells as a proportion of all

CD8⁺ T cells. **b**, IFN- γ responses of CD8⁺ T cells against EPT pools after one round of pre-stimulation measured by ICS pre-vaccination and at 16 weeks after vaccination. **c**, Bar graphs show absolute frequencies of EPT-pool-reactive CD8⁺ T cells producing one, two, or three cytokines. Pie charts summarize the fractions of the total CD8⁺ T-cell responses positive for one, two, or three cytokines. **d**, Median percentage cytokine production across six patients by CD8⁺ T cells after one round of pre-stimulation against EPT peptide pools.



Extended Data Figure 4 | Deconvolution of peptide pools to identify neoantigen-specific T-cell responses *ex vivo* against individual 15- to 16-mer ASP. Deconvolution of T-cell reactivity against individual ASP by *ex vivo* IFN- γ ELISPOT using the week 16 post-vaccination PBMCs, tested in duplicate or triplicate wells per peptide (error bars, s.e.m.). *Responses were scored positive if >55 spot-forming cells (SFC) were detected and were at least 1.5 s.d. over the DMSO control (>3 s.d. over background for patients

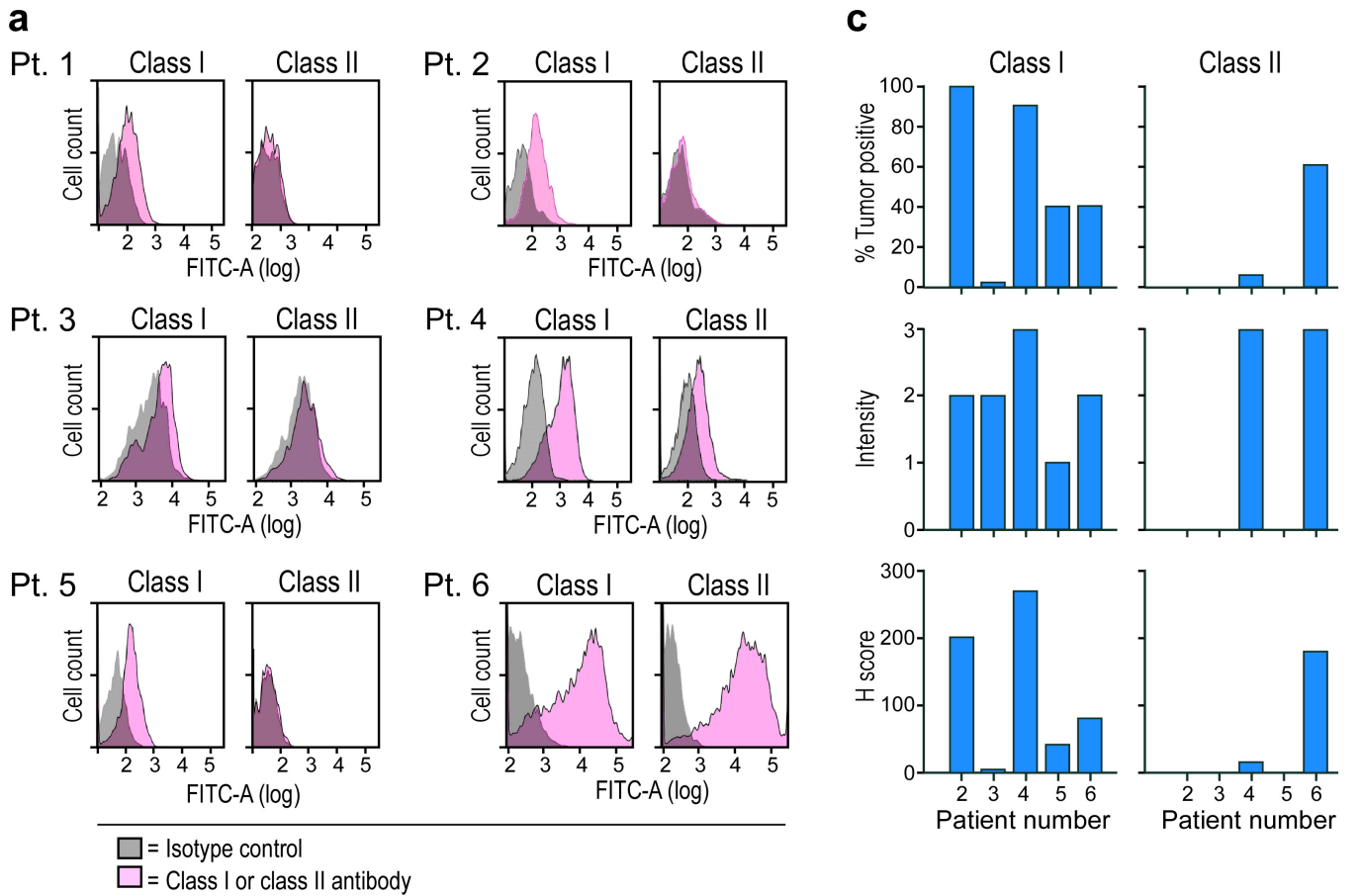
5 and 6). **a**, Patient 3 deconvolution. Inset: examples of positive IMP/ASP sequences; red, ASP stimulating reactivity; boxed, the mutated amino acids. **b**, Deconvolution for all other patients. **c**, IFN- γ ELISPOT response of patient 3 *CIT*-specific CD8⁺ T-cell line from week 16 (7×10^4 CD8⁺ T cells per well) against mutated (Mut) versus corresponding wild-type peptide across a range of concentrations (10 pg ml^{-1} to $10 \mu\text{g ml}^{-1}$) pulsed on 1×10^4 T-cell-depleted PBMCs (hereafter referred to as APCs) per well.



Extended Data Figure 6 | See next page for caption.

Extended Data Figure 6 | IFN- γ response of pre- and post-vaccination PBMCs against individual ASP, and IFN- γ response and CD107 $\alpha\beta$ degranulation by neoantigen-specific T-cell response against expressed minigenes. PBMCs from week 16 after vaccination were pre-stimulated with ASP and EPT for measuring CD4⁺ and CD8⁺ T-cell responses, respectively. **a**, Detection of IFN- γ responses by ELISPOT of CD4⁺ T cells against individual ASP after one round of pre-stimulation with ASP pools in matched pre- and 16-week post-vaccination samples for patients 1–6 (1×10^4 APCs and 1×10^4 T cells per well), tested in duplicate or triplicate wells per peptide (error bars, s.e.m.). **b**, Autologous B cells were nucleofected with *in vitro* translated RNA generated from mutated (Mut) or wild-type minigenes (MG). T-cell lines were cultured with mutated or wild-type minigene nucleofected B cells, mutated minigene nucleofected

B cells with anti-HLA class I or anti-HLA-DR antibodies, and non-nucleofected B cells with DMSO in IFN- γ ELISPOT (8×10^4 B cells per well were plated with 5×10^3 T cells per well and 1×10^4 CD8⁺ T cells per well for CD4⁺ and CD8⁺ T-cell response detection, respectively), tested in duplicate or triplicate wells per each condition (error bars, s.e.m.). **c**, T-cell lines were cultured with mutated minigene nucleofected B cells or non-nucleofected B cells followed by CD107 $\alpha\beta$ degranulation assay. Representative FACS plot of patient 3 CD107 $\alpha\beta$ degranulation assay for *VPS16*-specific CD8⁺ T-cell lines (top) and other neoantigen-specific CD4⁺ and CD8⁺ T-cell lines (bottom) from week 16 against autologous B cells nucleofected or not with mutated minigenes. FACS plots were pre-gated on CD8⁺ T cells.

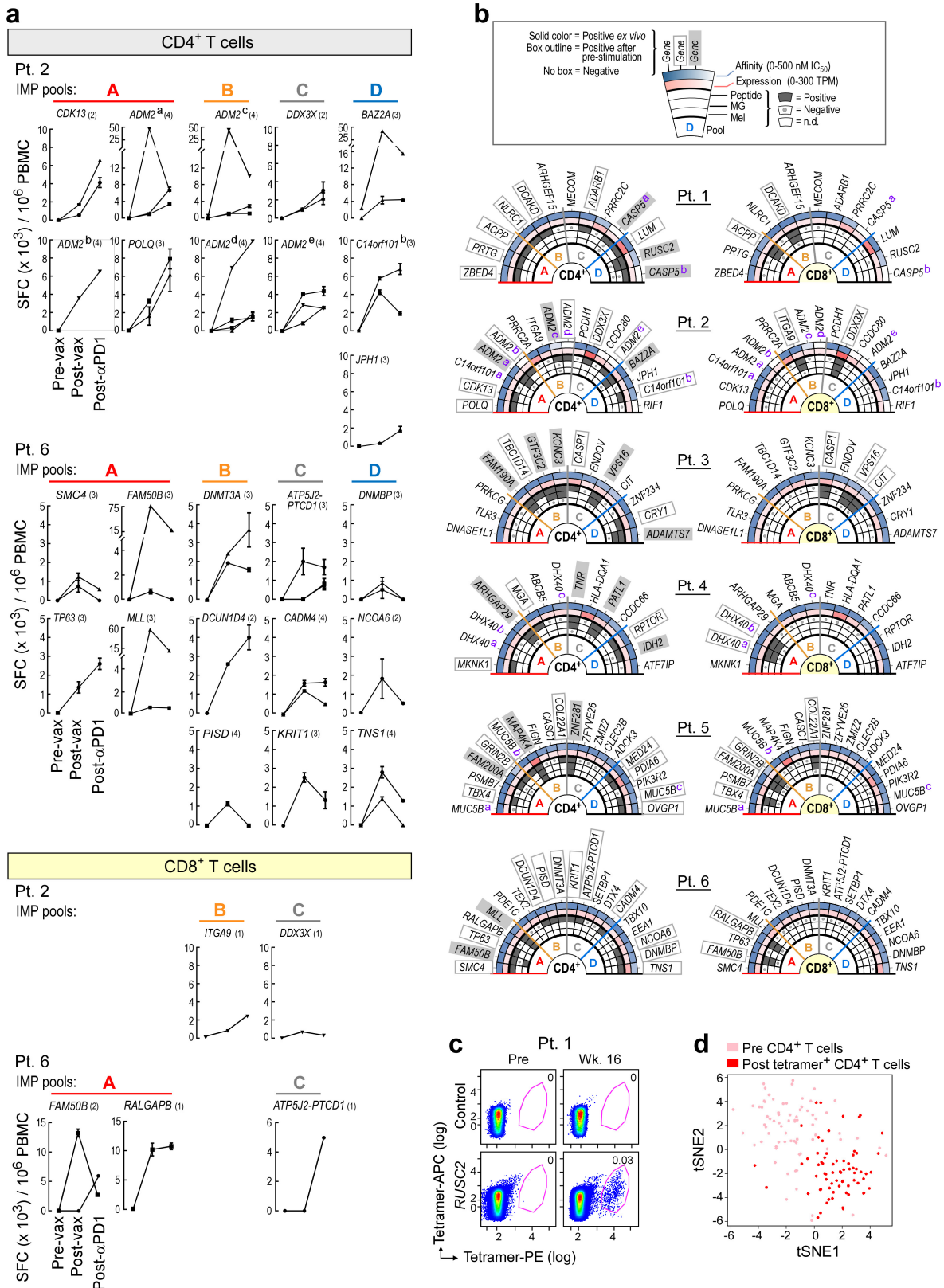


Extended Data Figure 7 | Surface expression of HLA class I and class II on patient melanoma cell lines and originally resected tumour.

a, Flow cytometric staining of autologous melanoma cell lines generated from primary tumour samples with anti-class I and anti-class II or isotype antibodies. **b**, Dual chromogenic immunohistochemical staining of excised FFPE tumours (see Methods for details). Representative images of positive staining for HLA class I (patients 4 and 2) and HLA class II (patient 6) and negative staining for class II (patient 2). Red, melanoma

transcription factor SOX10; brown, HLA class I or class II.

c, Summary of immunohistochemical results of five patients with available FFPE tissue. Semi-quantitative scoring was performed for the intensity of positive staining of melanoma cell membranes for class I or II (0, negative; 1, weak; 2, moderate; 3, strong) and for the percentage of positive staining malignant cells (0–100%). A cumulative *H* score was obtained by multiplying intensity score by the percentage of malignant cells with positive staining.



Extended Data Figure 8 | See next page for caption.

Extended Data Figure 8 | Repertoire of neoantigen-specific T-cell responses persists and broadens following PD-1 blockade, and summary of all CD4⁺ and CD8⁺ T-cell responses against neoantigens across the six patients. **a**, Persistent or new responses to mutated peptides after PD-1 blockade (pembrolizumab) are shown. PBMCs from patients 2 and 6 (before vaccination, week 16 after vaccination, or 11.5 months (patient 2) or 8.5 months (patient 6) after initiation of pembrolizumab therapy) were pre-stimulated for 21 days with ASP or EPT pools, and reactivity against individual ASP and EPT was then tested by IFN- γ ELISPOT. Ten thousand APCs per well were plated with 1×10^4 T-cell lines per well and 1×10^4 CD8⁺ T-cell lines per well for CD4⁺ and CD8⁺ T-cell response detection, respectively, tested in duplicate or triplicate wells per peptide (error bars, s.e.m.). Each line represents the IFN- γ response against a single ASP or EPT tested per immunizing

peptide. Number for each gene: total number of ASP or EPT tested per immunizing peptide. **b**, The rings, from outer to inner, show the following: (1) predicted affinity of peptide for HLA; heat map scaled from darkest (lowest half-maximal inhibitory concentration (IC₅₀) (nM), or highest affinity) to lightest (highest IC₅₀ (nM), or lowest affinity); (2) level of transcript expression of the tumour, scaled from darkest (highest number of transcripts per million reads) mapped to lightest (lowest number of transcripts per million reads); (3) reactivity to peptide-pulsed autologous APCs; (4) reactivity to B cells nucleofected with minigenes; (5) reactivity to cultured autologous melanoma cells. **c, d**, *Ex vivo* class II tetramer staining of patient 1 CD4⁺ T cells. Visualization of transcriptomes of single CD4⁺ T cells before vaccination and tetramer-positive CD4⁺ T cells after vaccination by *t*-distributed stochastic neighbour embedding (*t*-SNE).

Extended Data Table 1 | Characteristics of patients

Patient ID	Age	Gender	Primary site	Site of resected disease	Stage	Previous Treatment	Recurrence after NeoVax Y/N (Wks)
1	26	M	Back	Axillary LN	IIIC (T3bN3M0)	IFN α	N
2	68	F	Back	Lung	IVM1b (T4aN0M1b)	None	Y (*6, †28)
3	51	F	Left Calf	Skin - in transit	IIIC (T3bN2cM0)	None	N
4	56	M	Back	Axillary LN	IIIC (T4bN2bM0)	None	N
5	58	F	Left Arm	Skin	IIIC(T2aN2cM0)	None	N
6	61	M	Chest	Lung	IVM1b (T2aN0M1b)	IFN α	Y (*7, †20)
7	28	F	Unknown	Cervical LN	IIIB (TxN1bM0)	None	N/A
8	63	M	Back	Skin - Satellite Nodule	IIIB (T3aN2cM0)	None	N/A
9	71	M	Shoulder	Axillary LN	IIIB (T2aN1bM0)	IFN α	N/A
10	34	M	Right Foot	Femoral LN	IIIC (T4aN3M0)	None	N/A

M: male; F: female; LN: lymph node; N/A: not applicable; IFN α : Interferon alpha.

†: Weeks from vaccination initiation to further progression after vaccine.

*: Weeks from vaccination initiation to recurrence on vaccine.

■ Shaded: vaccinated patients.

Extended Data Table 2 | Class II tetramer information

Patient	Gene	Peptide sequence for tetramer	HLA allele	Predicted class II epitope sequence	Predicted percentile rank*
1	<i>RUSC2</i>	SVGDFSQEFSPIQEAQQD(K-dansyl)-amide	HLA-DRB1*04:01	SVGDFSQEFSPIQEA	2.16
			HLA-DRB1*04:01	DFSQEFSPIQEAQQD	5.77
4	<i>ARHGAP29</i>	PGKIHLFEEFTQVAKKE(K-dansyl)-amide	HLA-DRB1*01:01	LPGKIHLFEEFTQV	24.59
			HLA-DRB1*01:01	IHLFEEFTQVAKKE	28.84

*Consensus method in IEDB